Small, 6 (5), 687-694, 2010/**

Nitrogen and Luminescent Nitrogen-Vacancy Defects in Detonation Nanodiamond

Igor I. Vlasov, Olga Shenderova, Stuart Turner, Oleg I. Lebedev, Artem A. Basov, Ilmo Sildos, Mickel Rähn, Andrey A. Shiryaev, and Gustaaf Van Tendeloo*

***A**n efficient method to investigate the microstructure and spatial distribution of nitrogen and nitrogen-vacancy (N-V) defects in detonation nanodiamond (DND) with primary particle sizes ranging from approximately 3 to 50 nm is presented. Detailed analysis reveals atomic nitrogen concentrations as high as 3 at% in 50% of diamond primary particles with sizes smaller than 6 nm. A non-uniform distribution of nitrogen within larger primary DND particles is also presented, indicating a preference for location within the defective central part or at twin boundaries. A photoluminescence (PL) spectrum with well-pronounced zero-phonon lines related to the N-V centers is demonstrated for the first time for electron-irradiated and annealed DND particles at continuous laser excitation. Combined Raman and PL analysis of DND crystallites dispersed on a Si substrate leads to the conclusion that the observed N-V luminescence originates from primary particles with sizes exceeding 30 nm. These findings demonstrate that by manipulation of the size/nitrogen content in DND there are prospects for mass production of nanodiamond photoemitters based on bright and stable luminescence from nitrogen-related defects.*

Keywords:
- detonation nanodiamonds
- electron energy-loss spectroscopy
- nitrogen-vacancy defects
- photoluminescence
- Raman spectroscopy

[*] Dr. I. I. Vlasov, A. A. Basov
General Physics Institute, Russian Academy of Sciences
38 Vavilov Street, 119991 Moscow (Russia)
E-mail: vlasov@nsc.gpi.ru

Dr. O. Shenderova
International Technology Centre
8100-120 Brownleigh Drive, Raleigh, NC, 27617 (USA)

S. Turner, Dr. O. I. Lebedev, Prof. G. Van Tendeloo
EMAT, University of Antwerp
Groenenborgerlaan 171, 2020 Antwerp (Belgium)

Dr. I. Sildos, M. Rähn
Institute of Physics, University of Tartu
Riia Street 142, 51014 Tartu (Estonia)

Dr. A. A. Shiryaev
Institute of Crystallography RAS
Leninsky pr. 59, Moscow 119333 (Russia)

DOI: 10.1002/smll.200901587

1. Introduction

Nanodiamond (ND) particles belong to a broad family of nanocarbon-based materials with a structural diversity that is based on specific synthesis conditions, post-synthesis processes, and modifications.[1] ND particles with sizes up to several tens of nanometers currently find broad application in polishing, structural materials, and lubricants,[1] as well as prospective applications in biotechnology and medicine.[2] Recently, several important new application areas have been proposed based on the potential of incorporating foreign atoms and point defects into the nanoparticle lattice. Major breakthrough areas where controlled doping of NDs and on-demand production of nitrogen-vacancy (N-V) centers can revolutionize the field are quantum information processing and quantum computing,[3–5] nanoscale imaging magnetometry,[6] and photoluminescent probes.[7–12]

At the present time photoluminescent NDs (PL-NDs) with imaging, targeting, and therapeutic functionalities have been developed for biomedical applications, the most advanced field of use for doped ND particles.[2,7–12] Until now, the development of bright PL-NDs has focused on diamonds containing 10–300 ppm of native substitutional nitrogen, synthesized by static high-pressure high-temperature (HPHT) techniques.[7–12] The ND particles are obtained using a top-down approach by grinding larger, micrometer-sized particles. To produce PL-NDs, the NDs are irradiated with electrons, protons, He ions,[7–12] or other ions to create vacancies in the particle cores. Next, the ND is annealed in vacuum at 600–800 °C, which causes vacancy diffusion and formation of N-V centers emitting around 670 nm in the cores.

It is also possible to produce PL-NDs with green emission at 530 nm using natural diamond powders of type Ia. In this case the powders contain two substitutional N atoms in neighboring positions, producing N-V-N color complexes after irradiation and subsequent annealing.[9] For top-down synthesis of PL-ND both grinding of microscopic diamonds followed by irradiation to create N-V centers as well as the inverse method of inducing PL in microscopic diamonds followed by grinding[12] have been adopted. Importantly, stable PL from N-V defects created within ''single-digit'' (diameter less than 10 nm) NDs has been reported.[11,12]

Dynamic synthesis of NDs from the carbon contained in high-energy explosives (so called C-H-N-O explosives) is an alternative bottom-up approach for large-scale ND synthesis. These so-called detonation NDs have average primary particle sizes of approximately 3–6 nm, depending on the details of the synthesis, and possess a spherical/polyhedral shape.[1,2] A small fraction with larger sizes is also typically present in detonation ND (DND).[13] Currently, single-digit DND is produced at a kilogram level,[14] while production of single-digit ND from static synthesis is only just emerging.[11] Nitrogen is present in the mixture of initial explosive components used for detonation synthesis of diamond at a level of up to approximately 20 mass%,[1] however no information about its presence and form of incorporation in a DND core existed until recently. In general, DND is not seen as a potential material for the production of PL-ND based on creation of N-V centers,[12] although conjugation of DND with PL dyes useful for cell studies has been demonstrated,[2,15] as have fluorescent properties induced by DND surface functionalization.[2,16]

Difficulties in tracing the nitrogen in DND arise from the small sizes of the diamond crystallites and from the presence of a non-negligible fraction of surface atoms. The latter can easily be connected with different functional groups, including nitrogen-containing ones, during synthesis and purification. Progress in spatial resolution in microscale structural analysis techniques and new methodologies are helping investigators in gaining a step-by-step understanding of the peculiarities of nitrogen incorporation in NDs.

Recently incorporation of nitrogen into DND cores at a level of 2–3 at% was revealed using the scanning transmission electron microscopy electron energy-loss spectroscopy (STEM-EELS) technique.[13,17] To ensure that nitrogen atoms from surface groups did not contribute to the EELS signal, the DND surface was ''recreated''[13] by desorbing existing surface groups and transforming external diamond layers into sp^2 carbon by high-vacuum annealing, followed by sp^2 carbon removal using nitrogen-free liquid oxidizers. Time-resolved luminescence experiments[18] have shown that N-V centers can in principle be produced in DND, implying the presence of single-substituted nitrogen (N_s). In the same work N_s concentrations in DND were estimated by pulse electron paramagnetic resonance (EPR) at a level of 300 ppm. Weak EPR signals from the paramagnetic N_s have also been detected in DND after a HPHT sintering treatment.[19]

In the present work we have found very specific incorporation of nitrogen in typical DND. For the first time the existence of a strong PL with well-pronounced zero-phonon lines (ZPLs) at 575 and 638 nm, originating from the neutral ($(N\text{-}V)^0$) and negatively charged ($(N\text{-}V)^-$) N-V centers, has been demonstrated in DND particles using conventional PL spectroscopy without the need for a time-resolved technique. Using the ability of Raman analysis to estimate the size of a ND crystallite[20] we conclude that large diamond crystallites (larger than 30 nm) are the main source of the unperturbed N-V emission in DND (which is similar to that observed in bulk diamond).

2. Results

The size distribution of ND crystallites in the studied DND powder was analyzed by small-angle X-ray scattering (SAXS). The size distribution of the scatterers was obtained by assuming a spherical morphology using Tikhonov's regularization method[21] and is shown in Figure 1. The main peak in the particle size distribution corresponds to grains approximately 6 nm in diameter. The tail in the size distribution spreading beyond 25 nm reveals the presence of larger nanoparticles, indicating that the conditions of the explosive synthesis are not equal for all particles and that a small volume fraction of DND differs essentially in size from the main product. This fact was already pointed out previously.[22]

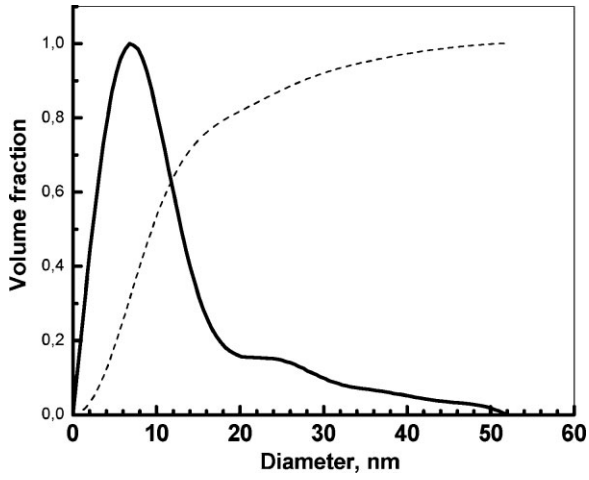

Figure 1. Size distribution (solid line) of the DND primary particles determined by SAXS. The main peak corresponds to grains of ≈6-nm diameter and the tail in the size distribution spreads beyond 25 nm. The dashed curve shows an integrated size distribution, that is, the volume fractions of the DND primary particles with sizes below a certain diameter.

NANO MICRO small

The crystal size of the dominant fraction determined by SAXS is larger than the 4-nm crystal size commonly determined by the X-ray diffraction (XRD) using the broadening of the Bragg peaks. This can be explained by the different principles used for crystal size determination in the two techniques. SAXS is based on the electron density contrast between the scatterer and the surrounding medium, thus providing information about the overall size of a ND particle. The width of the Bragg peaks in a XRD pattern reflect the size of so-called ''coherently scattering domains,'' which are usually smaller (rarely equal) than the entire particle size. For example, the XRD size of a twinned particle will correspond to the size of the individual untwinned sections, whereas the SAXS will give the size of the whole nanoparticle. The discrepancy in the crystal size determined by the two techniques suggests that there is a high concentration of twinned crystallites in the studied DND sample. High-resolution transmission electron microscopy (HRTEM) analysis (see below) confirms this conclusion.

Observations of DND crystallites in a HRTEM are consistent with the results obtained with SAXS. In the HRTEM images grain sizes of around 6 nm are typical (Figure 2a). Larger crystallites with sizes of 10–25 nm (Figure 2b) and exceptionally even of 100 nm (Figure 2c) are found. However, the fraction of smaller DND particles is also the most abundant.

ND particles up to approximately 6 nm often show twinning over coherent $\Sigma = 3\{111\}$ twin boundaries. The larger particles are mostly multiple-twinned DND particles, with up to 20 twin planes visible in a single particle (Figure 2b). Note that while SAXS averages information about the whole sample, TEM is highly local. The close correspondence of the SAXS and TEM results strongly indicates that the latter data are not seriously affected by sample preparation or limited statistics.

In earlier work[13] nitrogen impurity incorporation in the core of small diamond grains (below 6 nm) was evidenced using detailed EELS. In this study approximately 20% of the small (<6 nm) DND grains were found to contain a detectable amount of nitrogen embedded within the particle core. These statistics were obtained using an electron probe with a diameter of approximately 1 nm, so that some of nitrogen might have been missed when placing the probe on the core of larger DND particles (the goal of this earlier work was not to obtain statistical data). In the present work statistical data on the nitrogen incorporation in the smallest DND nanoparticles were obtained by studying 18 nanoparticles using a highly defocused electron probe, forming a larger probe that covers the entire core of each individual DND particle. Of the 18 nanoparticles studied using this technique, 50% showed a detectable nitrogen signal, indicating that nitrogen incorporation occurs in a larger amount of DND particles than previously thought.

The main purpose of the STEM-EELS analysis performed in this work was however to study the nitrogen content and nitrogen distribution within the larger diamond particles (>6 nm). For this reason a number of larger DND grains were traced using STEM-EELS, and a non-uniform distribution of nitrogen concentration within the grains was found. Two types of nitrogen-embedding were found to be predominant. In several nanoparticles nitrogen was localized in the central region of the DND core, indicating a preferred embedding at this central position. However, a preferential localization of nitrogen at twin boundaries was also detected.

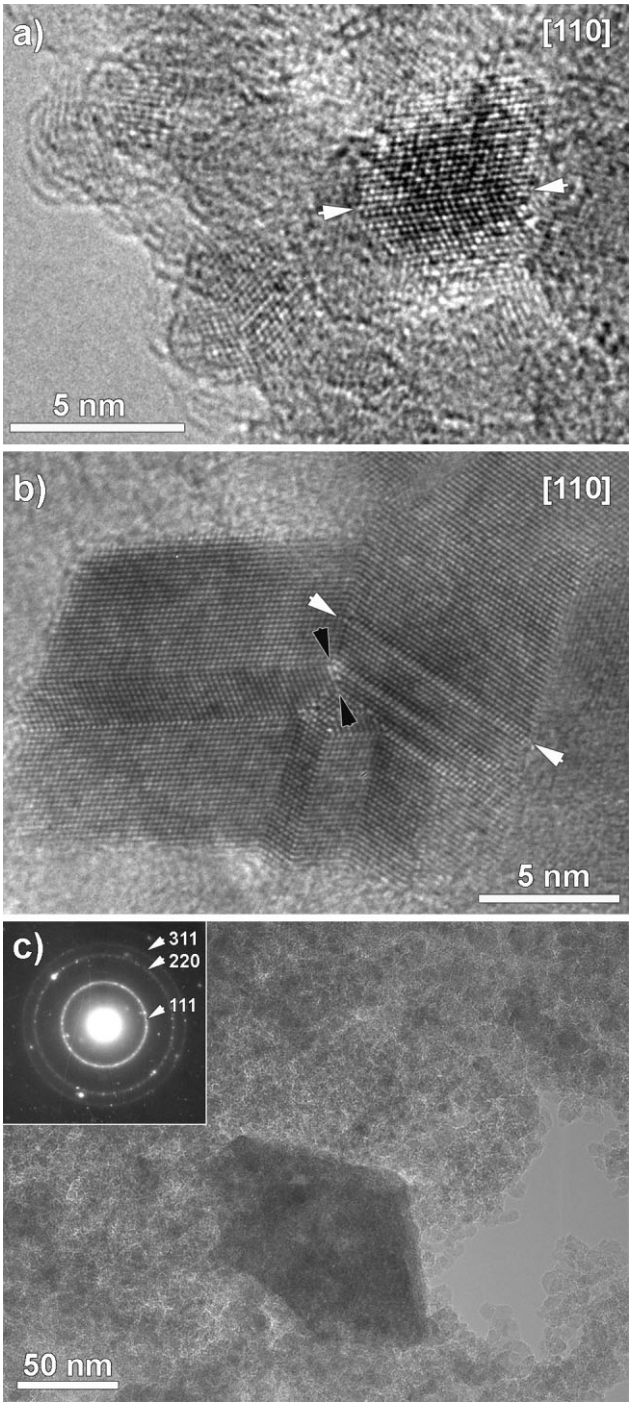

Figure 2. DND particle sizes. a) The main fraction of DND particles has a particle size close to 6 nm. Twinning is frequently observed in these small particles, with all visible twinning occurring over a {111} twin boundary (examples of twin planes are indicated by white arrows in a) and b)). b) Larger, multiple-twinned ND particle. An incoherent region is indicated by black arrows. c) A rarely observed 100-nm octahedral particle. The inset electron diffraction ring pattern is typical for all DND samples and clearly evidences the cubic diamond crystal structure of all of the nanoparticles.

A high-angle annular dark field (HAADF)-STEM image of a typical DND grain with ''central'' nitrogen localization is

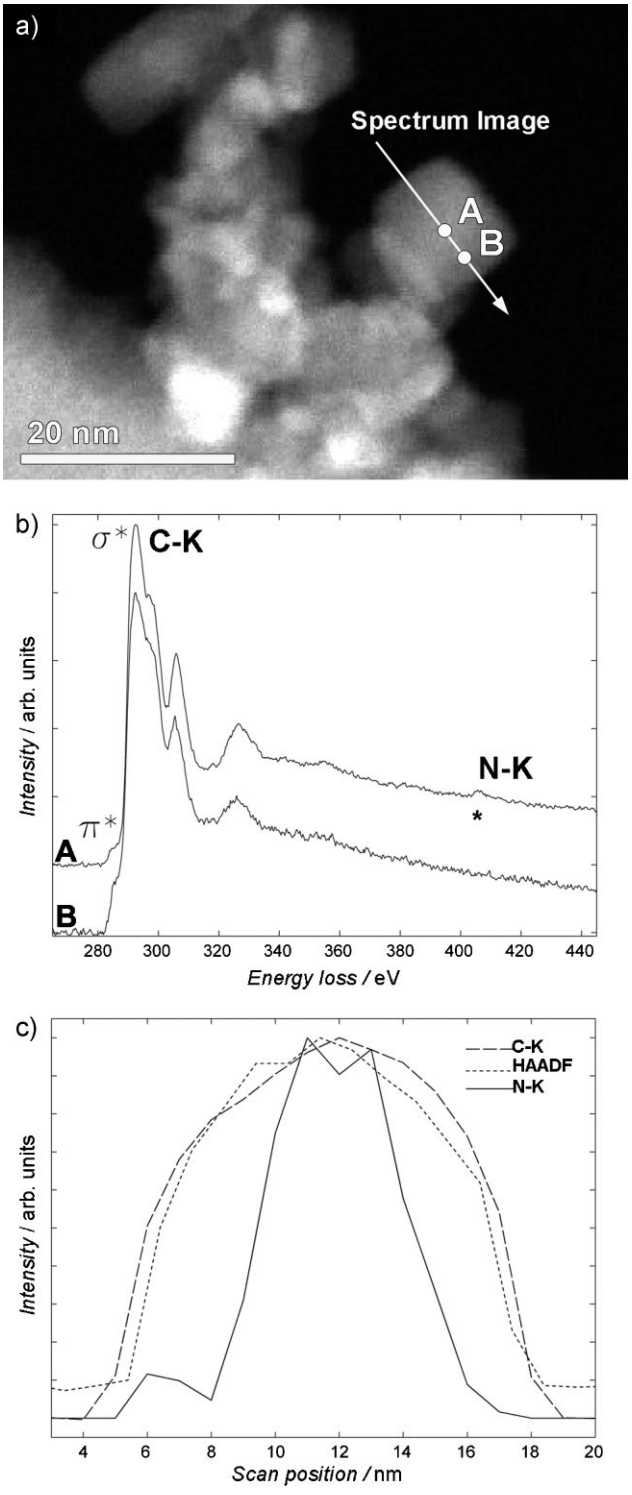

Figure 3. a) HAADF-STEM image of a large DND nanoparticle. The STEM-EELS 20-point line scan (spectrum image) is indicated in the image. b) Background-subtracted normalized EELS spectra from positions A and B from the large DND particle. The core region of the particle shows a clear nitrogen peak at 403 eV, the position closer to the surface (B) does not. c) Normalized nitrogen peak strength, carbon peak strength, and HAADF-STEM image intensity for the line scan from (a). The carbon strength follows the thickness profile (HAADF intensity). The particle is approximately 12 nm in diameter. Nitrogen is only detected within the inner 6 nm of the particle. The maximum N to C ratio (center of the particle) is 3.5 at%.

shown in Figure 3a. In total 20 EELS spectra were recorded in the line scan of the 12-nm grain. Two typical spectra — one at position A and one at position B on the particle — are displayed in Figure 3b. Both spectra show a carbon K-edge with σ^* contributions typical for diamond at 292 eV and π^* contributions at 285 eV arising from sp^2 hybridized surface carbon. Spectrum B also shows a larger graphitic π^* contribution, which is to be expected as a larger surface contribution is measured at the thinner position B. The spectrum at position A clearly shows a nitrogen signal at 403 eV (indicated by an asterisk), while the spectrum from position B does not. Using model-based quantifications methods[23–25] the nitrogen content was quantified over the whole line scan, and is plotted as the nitrogen signal strength together with the carbon signal strength and the HAADF-STEM signal intensity in Figure 3c.

The HAADF image intensity may be regarded as a thickness profile. It can be seen from the plot that there is only a detectable nitrogen signal within the inner 6 nm core of the DND particle. Towards the surface of the particle no nitrogen is detected. The maximum nitrogen content in the core of the particle was measured to be 3.5 at%. The lack of nitrogen signal towards the surface is not a result of signal noise, as can be seen when comparing spectrum A and B in Figure 3b.

An 18-nm DND grain with preferential nitrogen localization at a twin boundary is shown in Figure 4a. Two mutually perpendicular line scans (SI1 and SI2) were performed on the grain as demonstrated in Figure 4b. In total 20 EELS spectra were obtained in each scan. Five typical spectra — taken at positions A, B, C, D, and E — are displayed in Figure 4c. All spectra show a carbon K-edge with high diamond (σ^*) and small graphitic (π^*) contributions. Spectra A, B, and C as well as all spectra from the SI1 scan show a nitrogen signal at 403 eV (the nitrogen position is indicated by an asterisk). Spectra D and E from scan SI2 do not show any detectable N signal. Spectra D and E also show a larger graphitic π^* contribution due to increased surface sp^2 carbon at these positions. In order to quantify the average nitrogen content along the SI1 line, an average spectrum SI1 was calculated from spectra 5–16 of the first line scan (Figure 3c). The noise in the spectrum is significantly reduced by the averaging, and the nitrogen peak is clearly visible at 403 eV. The average nitrogen content was measured to be 3.5 at%.

The PL-Raman spectrum taken from a thick (about 1 mm) layer of DND powder is shown in Figure 5. The Raman part of the spectrum (see inset in Figure 5) consists of two lines at 1326 and 1630 cm^{-1} related to the vibrational modes of, respectively, diamond and sp^2-bonded carbon. For large (micrometer-scale and larger) crystals the diamond Raman peak is normally positioned at 1332 cm^{-1}, corresponding to the phonon modes from the center of the Brillouin zone, and has a symmetric shape. For nanoscale-sized crystals the diamond peak is down shifted from the 1332 cm^{-1} position and asymmetrically broadened with decreasing crystal size due to the phonon confinement effect.[26] The position of the diamond Raman line at 1326 cm^{-1} is expected to correspond to Raman scattering from the dominant fraction of 6-nm crystallites in the DND powder. The PL spectrum presents a structureless broad band with a maximum around 570 nm. As it was demonstrated that the characteristics of the ND PL can be strongly varied by

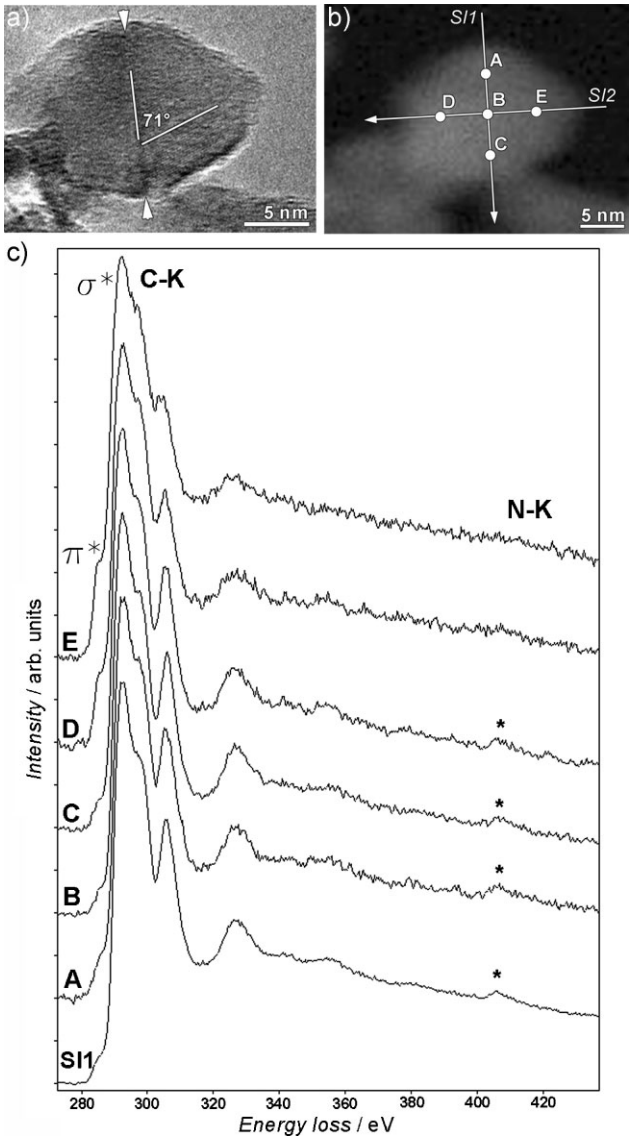

Figure 4. a) Bright-field TEM image showing a large DND particle with a twin boundary. The boundary is indicated by the two white arrows. b) HAADF-STEM image of the same large DND nanoparticle indicating the two 20-data-point line scans that were performed on the particle. SI1 was taken along the boundary, SI2 over the boundary. Five scan positions corresponding to five spectra in (c) are indicated by white dots. c) Background-subtracted, normalized EELS spectra from positions A, B, C, D, and E from the large DND particle. Spectra A, B, and C taken at the boundary show a nitrogen peak at 403 eV. Spectra D and E show no detectable nitrogen signals. Spectrum SI1 is the average spectrum of data points 5–12 taken on the DND particle in scan SI1. The nitrogen to carbon ratio in the averaged spectrum is 3.5 at%.

functionalization of the ND surface,[2,16,27] it is most likely that this broad PL band can be related to emission from electron levels created in the diamond bandgap by surface defects. No essential changes in the PL-Raman spectrum (not shown) of the thick DND layer took place after 2 MeV electron irradiation and 700 °C annealing of this material. When a thick layer of DND is used, the observed Raman and luminescence signals are expected to be mostly attributed to the main volume fraction of the diamond powder, consisting of approximately 6-nm crystallites.

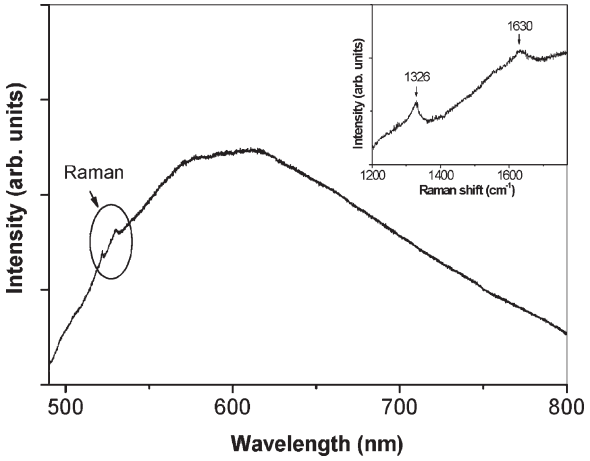

Figure 5. PL-Raman spectrum of DND powder measured at room temperature using a 488-nm excitation wavelength. The inset shows the Raman part of the spectrum in the range of 1200–1700 cm^{-1}. The PL spectrum presents a structureless broad band with a maximum around 600 nm. The Raman spectrum consists of the two lines at 1326 and 1630 cm^{-1} related to the vibrational modes of, respectively, diamond and sp^2-bonded carbon.

To increase the probability of detecting large diamond nanocrystals and to compare their PL spectra with those of 6-nm particles we applied the following procedure for DND sample preparation. The DND powder was dispersed in dimethyl sulfoxide (DMSO) and a thin DND layer was prepared on a Si substrate from this solution. A scanning electron microscopy (SEM) image of the DND layer is shown in Figure 6. The estimated thickness of the produced DND island-like layer was on average less than 100 nm. This allows measurement of the PL of the large diamond crystallites while minimizing interference from the small crystallites. Prior to the optical study the DND layer was electron-irradiated and annealed.

To study the PL properties of the layer a purpose-built PL-Raman spectroscopy system was used, working in 1) an image regime showing the integral PL intensity distribution within a large area of a sample surface, and 2) a regime of confocal PL-Raman spectra measurements. Using the first

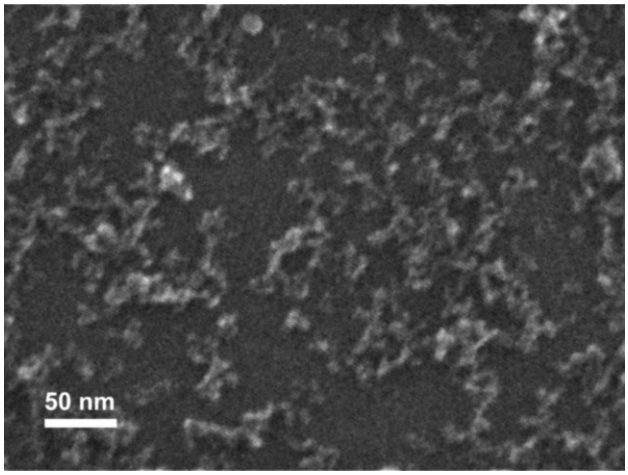

Figure 6. SEM image of DND crystallites dispersed on a Si substrate.

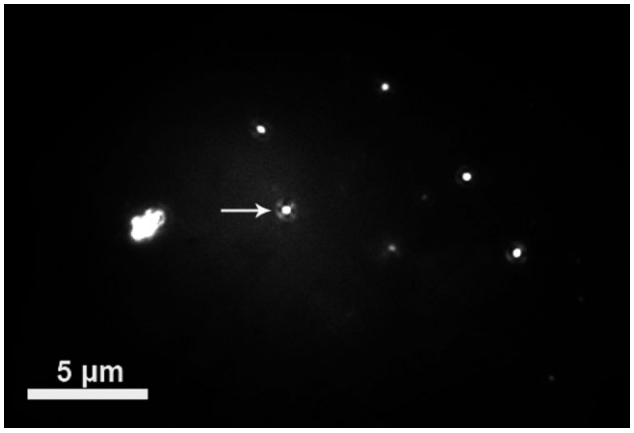

Figure 7. An image of the integral PL intensity distribution within a 532-nm laser spot ≈50 μm in diameter for DND crystallites dispersed on a Si substrate. The luminescence is selected by an edge filter passing light with wavelength >630 nm. A PL spectrum of the bright spot indicated by the white arrow is shown in Figure 8.

regime in combination with an edge filter (passing light with wavelength >630 nm), an image of the photoemission from the DND film surface illuminated with a 532 nm laser was obtained. This image, 53 μm ×37 μm in size, is shown in Figure 7.

A number of bright spots are clearly visible. A typical PL-Raman spectrum measured in one of the bright spots using the second regime is shown in Figure 8. Two lines at 575 and 638 nm, related to electron transitions at $(N\text{-}V)^{\circ}$ and $(N\text{-}V)^{-}$ defects are clearly visible in the spectrum. The diamond Raman line is detected in the unshifted 1332 cm^{-1} position, indicating that the bright emitting spots in Figure 7 are related to large DND crystals. According to Reference [20] a well-distinguishable down shift in the Raman position (about 2 cm^{-1}) from 1332 cm^{-1} is observable when the diamond particle size decreases below 30 nm. The lack of this shift in the Raman spectrum in Figure 8 leads to the conclusion that the bright PL from N-V centers is detected from DND crystallites with sizes

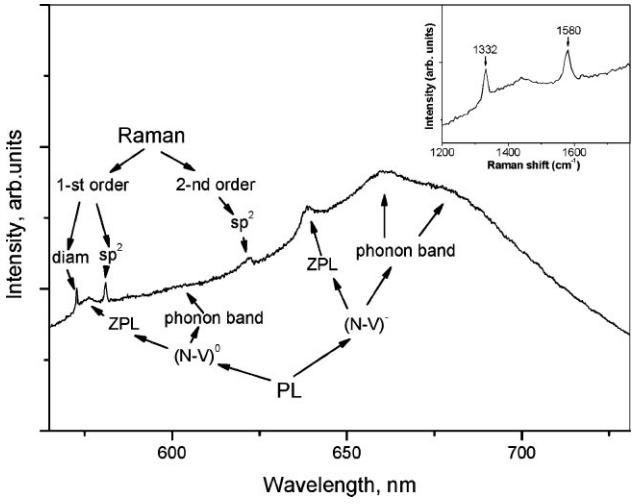

Figure 8. PL-Raman spectrum recorded at RT in the bright spot indicated by the white arrow in Figure 7. The insert shows the Raman part of the spectrum in the range of 1200–1700 cm^{-1}. The excitation wavelength is 532 nm. The laser beam is focused in a spot of 1-μm diameter.

above 30 nm. Besides the diamond Raman line, the first- and second-order Raman lines of sp^2-bonded carbon, and also the phonon sidebands of the $(N\text{-}V)^{\circ}$ and $(N\text{-}V)^{-}$ centers, are observed in the PL-Raman spectrum (Figure 8).

3. Discussion

In our previous work[13] the nitrogen concentration in a large amount of small DND crystallites (6 nm and below) was accurately quantified by spatially resolved EELS in combination with model-based quantification techniques. Nitrogen concentrations as high as 3 at% nitrogen were found in the core of approximately 20% of the analyzed grains. Further work using a larger, defocused electron probe showed a detectable nitrogen signal in 50% of the studied DND particles below 6 nm.

To study the distribution of nitrogen inside the larger DND grains, detailed EELS scans with 1-nm spatial resolution were carried out on several larger DND crystallites. A non-uniform distribution of the nitrogen, together with local high (3.5 at%) nitrogen concentrations, has been demonstrated. Such a spatially localized high-level incorporation of nitrogen is assumed to be related to the frequent occurrence of twins and multiple twin boundaries in DND crystallites. This multiple twinning also leads to the appearance of incoherent regions within diamond nanocrystals (Figure 2b). The incoherent regions are rich in structural defects (dangling bonds and other defects) and can be sources of high local strain.[28,29] Since the nitrogen atomic volume is 40% larger than that of carbon grain boundaries, twin boundaries and regions with high tensile stress favor nitrogen accumulation. This accumulation at defects and boundaries is made clear by the results presented in Figure 4. The two line scans performed on the DND particle clearly show an accumulation of nitrogen with a high concentration (3.5 at%) at the twin boundary between two primary diamond grains.

The existence of regions with high nitrogen concentrations in DND raises questions about the dominant structural form of N in those regions. Observation of the nitrogen K-edge onset at 403 eV in the EELS spectra from a large DND, combined with data from other methods, brings useful information about the possible structural forms of nitrogen in DND. Detailed examination of the N K-edge onset in Ia natural diamond[30] showed that the electron energy-loss near edge structure (ELNES) feature of the nitrogen K-edge at 403 eV in the EELS spectra is characteristic for substitutional nitrogen impurities in diamond. Under EPR examination, paramagnetic single-substitutional nitrogen (the P1-defect) shows a weak signal in DND, thus excluding the possibility of there being a significant fraction of this defect in DND.[18,19,31,32] Effective charge compensation of the nitrogen donor is unlikely to explain the weakness of the P1 EPR signal. According to multiple scattering theory modeling[30] the K-edge onset of positively charged substitutional nitrogen (N^{+}) would be observed at considerably higher energy than 403 eV (positive chemical shift). Recent NMR spectroscopy examination of N^{15} in DND concluded that the majority of the nitrogen defects in DND have a structure without unpaired electrons, that is, trigonal C–N bonding with a lone electron pair on the

NANO MICRO small

nitrogen.[33] A structure without unpaired electrons could be formed by binding nitrogen to only three carbons at a defective boundary. The requirement of the absence of a lone electron pair for a nitrogen atom in diamond bulk requires N aggregation. The best known non-paramagnetic N defects are a pair of neighboring substitutional N atoms (the A center)[34] and a group of four nitrogen atoms around a vacancy (the B center).[35] These nitrogen complexes are characteristic of nitrogen-containing natural diamond.

IR absorption spectroscopy is a typical technique used to detect the presence of A and B defects in diamond. This technique is, however, not useful for the characterization of bulk defects in DND because of strong scattering of the probing light and intense absorption by various groups on the diamond surface in the 1000–1300 cm^{-1} spectral range, overlapping with the bands due to A and B defects. Both of these centers can, however, be detected indirectly if they couple with vacancies (V). The resulting defects, known as H3 (A+V) and H4 (B+V) centers, are identified in PL and absorption spectroscopy by ZPLs at 503.2 and 496.2 nm, respectively. Neither our experiments (not shown) nor the literature data reveal the presence of such H3 and H4 defects in PL or absorption. Most likely none of the known optically active nitrogen complexes are formed in detectable amounts in DND, and the nitrogen in DND forms larger nitrogen complexes that are optically inactive.

The bright emission from N-V centers was found mainly in less defective large ND crystallites, revealing the presence of nitrogen in a single substitutional form. However this finding does not indicate the absence of N-V centers in smaller particles. Many factors like interactions with structural defects and with regions of highly localized nitrogen or strong broadband PL from surface defects could prevent an observation of N-V emission in small DND crystallites. An average of approximately 40 carbon bonding defects inside a 4.8-nm DND particle were revealed by NMR spectroscopy,[33] meaning that intensive formation of structural defects is an intrinsic feature of DND synthesis. This fact imposes constraints on the production of efficiently luminescent centers in 5-nm DND. Note that N-V PL has already been demonstrated for ND with sizes of 10 nm and smaller, produced by grinding of microscopic HPHT diamond.[11,12] This ND is in principle far less defective than DND particles. However, even in that case the N-V band observed in the PL spectrum was structureless and the band maximum was shifted from its typical position at 670 to 700 nm.[12] Therefore, such important characteristics as the high spectral selectivity of N-V emission supplied by narrow ZPLs are lost in 10-nm ND, whereas the ND crystallites with sizes larger than 30 nm demonstrate N-V PL with well-pronounced ZPLs (4-nm line width at room temperature (RT)).

4. Conclusion

The non-uniform distribution of high nitrogen concentrations (up to 3.5 at%) in large DND was demonstrated by a detailed EELS analysis. In most nanoparticles the nitrogen is localized in the central region of the particle core. Such a spatially localized high-level incorporation of nitrogen is assumed to take place in regions with a defective structure. An excess of nitrogen is also detected at twin boundaries in some nanoparticles. Combined Raman and PL spectroscopy of DND revealed emission from $(N\text{-}V)^{\circ}$ and $(N\text{-}V)^{-}$ centers in the large crystallites after electron irradiation and annealing of the DND material. It had long been thought that N could not be incorporated into DND cores at all, forming defects only at the surface of the diamond particles. The results of this work lead to the conclusion that ND with intense and stable emission from N-V centers can be produced by detonation synthesis of large diamond crystallites (>30 nm). The large DND grains can be separated from DND powder produced by a conventional detonation method or can be produced at modified synthesis conditions.

5. Experimental Section

Materials: The ND used in this work was purchased from New Technologies, Chelyabinsk, Russia. The ND particles were synthesized by the detonation of a mixture of trinitrotoluene (TNT) and hexogen (40:60) in an ice-cooling medium, followed by a soot purification process using a mixture of sulfuric acid and chromic anhydride, washing with deionized (DI) water, and drying. The sample was additionally purified from metal impurities by boiling in a $NaOH/H_2O_2$ mixture followed by washing in DI water, treating with ion-exchange resins, and drying. Subsequently the powder was dispersed in DMSO and fractioned by centrifugation to the slurry with average aggregate size of 60 nm. This fraction of DND was also depleted of small primary particle sizes using centrifugation. The incombustible impurity content in the final DND product was 0.5 wt%. The elemental composition measured using a Carlo Erba EA 1108 CHNS Analyzer was C 86.2, H 0.5, N 2.5 wt%. DND was dispersed over a Si substrate by immersing the substrate in a slurry of a DND in DMSO/methanol (1:3) followed by treatment for 10 min in an ultrasonic bath.[36] After ultrasonic treatment the substrate was rinsed with methanol and dried. For the production of N-V defects in both the DND powder and the DND thin film on Si substrate, the samples were irradiated by 2 MeV electrons at a dose of 5×10^{18} cm^{-2} and annealed at 700 °C for 1 h in vacuum.

TEM and EELS: TEM, HRTEM, and electron diffraction (ED) experiments were performed on a JEOL 4000EX microscope operated at 400 kV with a point resolution of 0.17 nm. STEM-EELS experiments were performed on a JEOL 3000F TEM/STEM microscope, equipped with a GIF-2000 spectrometer. The STEM-EELS spectra were acquired using a convergence semi-angle α of 10 mrad, a collection semi-angle β of 29 mrad, a nominal spot size of 1 nm, an energy dispersion of 0.3 eV per pixel, and an energy resolution of ≈1.2 eV. All core-loss spectra were background-subtracted, aligned using the onset of the carbon K-edge (at 284 eV), and normalized in intensity to their maxima. The nitrogen to carbon ratio (at% N) was obtained by model-based quantification of the acquired spectra. To model the core-loss spectra using the EELSMODEL software a power-law background AE^{-r} was used. The carbon K-edge and nitrogen K-edge were modeled using a hydrogenic atomic cross section. Both edges were topped with an equalization function to mimic the density of states. The model

was fitted using the Levenberg–Marquardt method for Poisson statistics.

PL and Raman spectroscopy: PL-Raman spectra of DND powder sample were recorded at RT using a LABRAM HR spectrometer with an Ar^+ laser for excitation. The laser radiation of 1-mW power at 488-nm wavelength was focused to a spot of 2-μm diameter on the surface of the DND samples. A purpose-made setup was built based on an inverted microscope (Olympus MX14), where at wide-field excitation an image of fluorescent DND particles dispersed over a Si substrate was recorded by a matrix detector Newton EMCCD (Andor). Radiation at 532 nm of a CW Nd:YAG laser VA-532 was used for the wide-field excitation of the emitting DND particles. To obtain PL-Raman spectra of single DND particles, the emission was dispersed by a spectrometer (Andor 303) equipped with a CCD camera. The backscattered laser light was blocked by a holographic Super Notch filter HSPF-532.0-1.0 (Kaiser). To avoid an exposure during the EMCCD image readout, an electromechanical shutter was installed in front of the camera.

SAXS: SAXS was performed using a dedicated laboratory AMUR-K diffractometer with position sensitive detector. A Kratki collimation scheme was employed. The size distribution of the particles was calculated assuming spherical shapes using Tikhonov's regularization method (GNOM software).[21]

Acknowledgements

Dr. S. Hens, V. Borganovich, and G. McGuire are acknowledged for helpful discussion. Dr. T. Tyler is acknowledged for taking the SEM (Figure 6) image. Financial support was provided by the Russian Foundation for Basic Researches, grants 08-02-01306 and 08-05-00745, and the European Union Framework 6 program under a contract from an Integrated Infrastructure Initiative (Reference 026019 ESTEEM).

[1] *Ultrananocrystalline Diamond*, (Eds: O. Shenderova, D. Gruen), William-Andrew, Norwich, NY **2006**.
[2] A. M. Schrand, S. C. Hens, O. A. Shenderova, *Crit. Rev. Solid State Mater. Sci.* **2009**, *34*, 18.
[3] P. Neumann, N. Mizuochi, F. Rempp, P. Hemmer, H. Watanabe, S. Yamasaki, V. Jacques, T. Gaebel, F. Jelezko, J. Wrachtrup, *Science* **2008**, *320*, 1326.
[4] V. Jacques, E. Wu, F. Grosshans, F. Treussart, P. Grangier, A. Aspect, J.-F. Roch, *Science* **2007**, *315*, 966.
[5] N. B. Manson, J. P. Harrison, M. J. Sellars, *Phys. Rev. B* **2006**, *74*, 104303.
[6] G. Balasubramanian, I. Y. Chan, R. Kolesov, M. Al-Hmoud, J. Tisler, C. Shin, C. Kim, A. Wojcik, P. R. Hemmer, A. Krueger, T. Hanke, A. Leitenstorfer, R. Bratschitsch, F. Jelezko, J. Wrachtrup, *Nature* **2008**, *455*, 648.
[7] O. Faklaris, D. Garrot, V. Joshi, F. Druon, J.-P. Boudou, T. Sauvage, P. Georges, P. Curmi, F. Treussart, *Small* **2008**, *4*, 2236.
[8] Y.-R. Chang, H.-Y. Lee, K. Chen, C.-C. Chang, D.-S. Tsai, C.-C. Fu, T.-S. Lim, Y.-K. Tzeng, C.-Y. Fang, C.-C. Han, H.-C. Chang, W. Fann, *Nat. Nanotechnol.* **2008**, *3*, 284.
[9] V. Vaijayanthimala, H.-C. Chang, *Nanomedicine* **2009**, *4*, 47.
[10] Y. Sonnefraud, A. Cuche, O. Faklaris, J.-P. Boudou, T. Sauvage, J.-F. Roch, F. Treussart, S. Huant, *Opt. Lett.* **2008**, *33*, 611.
[11] J. Tisler, G. Balasubramanian, B. Naydenov, R. Kolesov, B. Grotz, R. Reuter, J.-P. Boudou, P. A. Curmi, M. Sennour, A. Thorel, M. Borsch, K. Aulenbacher, R. Erdmann, P. R. Hemmer, F. Jelezko, J. Wrachtrup, *ACS Nano* **2009**, *3*, 1959.
[12] J.-P. Boudou, P. A. Curmi, F. Jelezko, J. Wrachtrup, P. Auber, M. Sennour, G. Balasubramanian, R. Reuter, A. Thorel, E. Gaffet, *Nanotechnology* **2009**, *20*, 235602.
[13] S. Turner, O. I. Lebedev, O. Shenderova, I. I. Vlasov, J. Verbeeck, G. Van Tendeloo, *Adv. Funct. Mater.* **2009**, *19*, 2116.
[14] E. Osawa, *Diamond Relat. Mater.* **2007**, *16*, 2018.
[15] S. C. Hens, G. Cunningham, T. Tyler, S. Moseenkov, V. Kuznetsov, O. Shenderova, *Diamond Relat. Mater.* **2008**, *17*, 1858.
[16] V. N. Mochalin, Y. Gogotsi, *J. Am. Chem. Soc.* **2009**, *131*, 4594.
[17] A. V. Kvit, V. V. Zhirnov, T. Tyler, J. J. Hren, *Composites, Part B* **2004**, *35*, 163.
[18] B. R. Smith, D. W. Inglis, B. Sandnes, J. R. Rabeau, A. V. Zvyagin, D. Gruber, C. J. Noble, R. Vogel, E. Ōsawa, T. Plakhotnik, *Small* **2008**, *5*, 1649.
[19] P. G. Baranov, I. V. Il'in, A. A. Soltamova, A. Ya. Vul,' S. V. Kidalov, F. M. Shakhov, G. V. Mamin, S. B. Orlinskii, M. K. Salakhov, *JETP Lett.* **2009**, *89*, 409.
[20] Z. Sun, J. R. Shi, B. K. Tay, S. P. Lau, *Diamond Relat. Mater.* **2000**, *9*, 1979.
[21] M. I. Svergun, *J. Appl. Crystallogr.* **1992**, *25*, 495.
[22] V. L. Kuznetsov, M. N. Aleksandrov, I. V. Zagoruiko, A. L. Chuvilin, E. M. Moroz, V. N. Kolomiichuk, V. A. Likholobov, P. M. Brylyakov, G. V. Sokovich, *Carbon* **1991**, *29*, 665.
[23] The program is freely available under the GNU public license and it can be downloaded from http://www.eelsmodel.ua.ac.be (accessed December 2009).
[24] J. Verbeeck, S. Van Aert, *Ultramicroscopy* **2004**, *101*, 207.
[25] G. Bertoni, J. Verbeeck, *Ultramicroscopy* **2008**, *108*, 782.
[26] J. W. Ager, III, D. K. Veirs, G. M. Rosenblatt, *Phys. Rev. B* **1991**, *43*, 66491.
[27] S. Hu, F. Tian, P. Bai, S. Cao, J. Sun, J. Yang, *Mater. Sci. Eng. B* **2009**, *157*, 11.
[28] A. H. King, F. R. Chen, L. Chang, J. J. Kai, *Interface Sci.* **1997**, *5*, 287.
[29] O. A. Shenderova, D. W. Brenner, *Phys. Rev. B* **1999**, *60*, 7053.
[30] R. Brydson, L. M. Brown, J. Bruley, *J. Microsc.* **1998**, *189*, 137.
[31] M. E. Newton, J. M. Baker, *J. Phys.: Condens. Matter* **1989**, *1*, 9801.
[32] A. Banaszak, K. Fabisiak, M. Kaczmarski, M. Kozanecki, *Cryst. Res. Technol.* **2006**, *41*, 535.
[33] X. Fang, J. Mao, E. M. Levin, K. Schmidt-Rohr, *J. Am. Chem. Soc.* **2009**, *131*, 1426.
[34] G. Davies, *J. Phys. C* **1976**, *9*, L537.
[35] R. Jones, P. R. Briddon, S. Oberg, *Philos. Mag. Lett.* **1992**, *66*, 67.
[36] O. Shenderova, S. Hens, G. McGuire, *Diamond Relat. Mater.*, DOI: 10.1016/j.diamond.2009.10.008.

Received: August 24, 2009
Revised: November 11, 2009
Published online: January 27, 2010

